Effect of Small Focus on Electron Heating and Proton Acceleration in Ultrarelativistic Laser-Solid Interactions

N. P. Dover[1,*] M. Nishiuchi,[1,2] H. Sakaki,[1] Ko Kondo,[1] M. A. Alkhimova,[3] A. Ya. Faenov,[4,3] M. Hata,[5]
N. Iwata,[5] H. Kiriyama,[1] J. K. Koga,[1] T. Miyahara,[1,6] T. A. Pikuz,[4,3] A. S. Pirozhkov,[1] A. Sagisaka,[1]
Y. Sentoku,[5] Y. Watanabe,[6] M. Kando,[1] and K. Kondo[1]

[1]*Kansai Photon Science Institute, National Institutes for Quantum and Radiological Science and Technology,
Kizugawa, Kyoto 619-0215, Japan*
[2]*PRESTO, Japan Science and Technology Agency, 4-1-8 Honcho, Kawaguchi, Saitama 332-0012, Japan*
[3]*Joint Institute for High Temperatures, Russian Academy of Sciences, Moscow 125412, Russia*
[4]*Open and Transdisciplinary Research Initiative, Osaka University, Suita, Osaka 565-0871, Japan*
[5]*Institute of Laser Engineering, Osaka University, 2-6 Yamadaoka, Suita, Osaka 565-0871, Japan*
[6]*Interdisciplinary Graduate School of Engineering Sciences, Kyushu University, Kasuga, Fukuoka 816-8580, Japan*

Acceleration of particles from the interaction of ultraintense laser pulses up to 5×10^{21} W cm^{-2} with thin foils is investigated experimentally. The electron beam parameters varied with decreasing spot size, not just laser intensity, resulting in reduced temperatures and divergence. In particular, the temperature saturated due to insufficient acceleration length in the tightly focused spot. These dependencies affected the sheath-accelerated protons, which showed poorer spot-size scaling than widely used scaling laws. It is therefore shown that maximizing laser intensity by using very small foci has reducing returns for some applications.

The interaction of high intensity laser pulses with solid targets is fundamental to many applications of high power lasers including energetic ion and x-ray sources [1–3], fast ignition inertial confinement fusion [4–6], radiobiology [7,8], materials science [9,10], and others [11,12]. Progress in high power laser technology [13] has recently enabled experimental investigation at intensities approaching the radiation-reaction dominated and QED regime [14], and facilities are coming online to demonstrate applications based on such interactions.

When ultraintense lasers (normalized vector potential $a_0 \gg 1$) interact with solids, electrons are accelerated to relativistic energies by the extreme laser fields [15,16]. Estimating the electron energy is complicated by field patterns generated by the focusing and reflected laser [17], plasma fields [18,19], and prepulse induced preplasma [20,21]. A commonly used scaling law to predict the increase in electron temperature, T_e, with laser intensity I_L is the ponderomotive scaling $T_{\text{pond}} = (\gamma_t - 1)m_e c^2$, where $\gamma_t = \sqrt{(1 + a_0^2)}$, the maximum transverse kinetic energy in

a plane wave [15]. However, other theories based on energy conservation [22], time-averaged momentum [16], and empirical scalings [23] predict worse scaling. The scaling of this and other electron parameters to ultrahigh intensities is not clear, particularly in the ∼fs pulse regime.

One key application of electron heating is target normal sheath acceleration (TNSA), or sheath acceleration, of ions [24–27]. Although other acceleration mechanisms have been investigated such as radiation pressure acceleration [28,29], collisionless shockwave acceleration [30–32], and relativistically induced transparency or breakout afterburner [33–35], sheath acceleration is attractive for applications due to its simplicity, robustness, and smooth beam profile. Electrons propagate through a thin foil, generating a quasielectrostatic field on the target surface which accelerates ions. Various acceleration models predict ion energies based on electron flux, temperature, and divergence [36–45]. To understand model efficacy, experimental studies on laser-electron coupling and ion acceleration at the high intensity frontier are crucial for realizing the potential of next generation high power lasers.

In this Letter, we investigate the laser intensity scaling of electron and proton acceleration in laser-solid interaction up to $I_L \approx 5 \times 10^{21}$ W cm^{-2} ($a_0 \approx 50$). We demonstrate that electron temperature depends not only on laser intensity, but also on focal spot size, which restricts the electron acceleration length and therefore temperature.

We find reduced electron divergence for tightly focused laser pulses due to beam generated magnetic fields in the preplasma. We demonstrate that the resultant sheath accelerated proton energies increase only modestly with decreased focal size due to reducing acceleration time. Increasing laser energy, not just laser intensity, may be the only route for achieving significant increase to maximum proton energies without employing more sophisticated acceleration schemes.

An $f/1.4$ off-axis parabolic mirror focused the 0.1 Hz, $\tau_L \approx 40$ fs, $E_L \approx 10$ J (on target), $\lambda_L \approx 800$ nm J-KAREN-P laser [46–48] to a focal size $r_L \approx 1.5$ μm (FWHM), resulting in a peak $I_L = 5 \times 10^{21}$ W cm^{-2}, measured at full power [46]. A motorized tape provided a $d = 5$ μm thick stainless steel foil at 45° to the p-polarized laser. The intensity was controlled by reducing E_L or moving the target with respect to the laser focus, measuring I_L at the offset. This setup allowed accumulation of a relatively large dataset compared to that typically used in ultrahigh intensity laser-solid interaction experiments ($\sim$100 shots).

The experiment is shown in Fig. 1(a) [49]. The electron spectrum is measured along the laser axis using a magnetic spectrometer with a phosphor scintillator (Mitsubishi DRZ), and the electron beam spatial profiler used another scintillator filtered by 6 mm polytetrafluoroethylene, eliminating ions, and < 2 MeV electrons. The proton spectrum was measured along target normal with a time-of-flight (TOF) diagnostic with 5 m drift length [56], with a scintillator-based proton beam profile monitor ensuring target normal pointing [59]. Radiochromic film (RCF) stacks could be inserted for high dynamic range spatially resolved spectroscopy [60], confirming the TOF measurement.

The laser prepulse causes pre-expansion of the target, affecting the main pulse interaction. The laser contrast was measured using a third order cross-correlator, and its effect on the target was calculated using FLASH [49]. The axial density profile 10 ps before the main pulse is shown in Fig. 1(b) for different laser conditions, showing a characteristic double scale length transitioning near the critical density $n_c \approx 10^{21}$ cm^{-3} where the prepulse is strongly absorbed. Because of transverse heat transport, a small variation of laser parameters does not significantly affect the
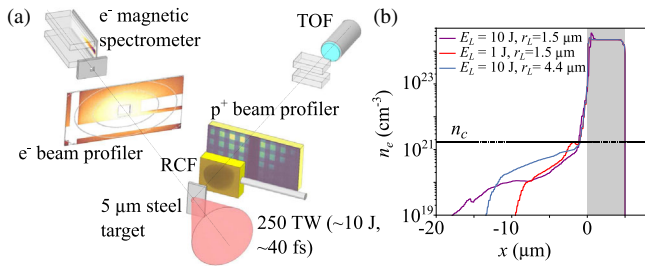
preplasma. In the preplasma, the proportion of contaminant protons to ions is less than a few percent, and therefore front side acceleration is dominated by the more abundant target ions, resulting in inefficient acceleration [58].

Typical electron spectra are shown in Fig. 2(a) for three shots: $I_L \approx 5 \times 10^{21}$ W cm^{-2}, and reduced intensity $I_L \approx 6 \times 10^{20}$ W cm^{-2} by defocusing ($r_L \approx 5$ μm), or reducing energy ($r_L \approx 1.5$ μm). At the highest intensity, the high energy tail has a temperature $T_e \approx 12$ MeV [least square fitting of $dN/dE \propto \exp(E/T_e)$ at $E > 7$ MeV], significantly lower than $T_{pond} \approx a_0 m_e c \approx 24$ MeV predicted from the ponderomotive theory. When I_L is reduced by increasing r_L at fixed energy, the $T_e \approx 9$ MeV is close to the ponderomotive scaling prediction $\approx$8 MeV. Unexpectedly, for the same I_L but a smaller r_L, T_e is reduced to $\approx$5 MeV. The temperature not only depends on I_L, but also r_L. Data from a single shot sequence in which the energy and focal spot were varied are shown in Fig. 2(b). Although T_e follows ponderomotive scaling at low intensities, it is suppressed as the intensity increases. Furthermore, suppression is more significant for the small r_L used when varying E_L.

A typical electron beam spatial profile is shown in Fig. 2(c) at highest intensity. The electrons are directed near laser axis with divergence $\theta_e \approx 30°$ (FWHM), similar
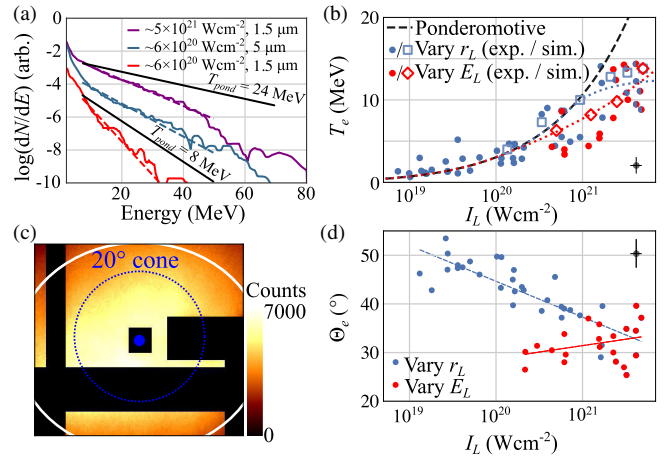

FIG. 2. (a) Electron spectrum for best focus full energy (purple), larger focus full energy (blue), best focus reduced energy (red), T_e fits (dashed), and ponderomotive prediction T_{pond} (black). (b) Experimental measurements of T_e against I_L by changing r_L (blue circles), or E_L at best focus (red circles), typical uncertainty (black cross) and respective PIC results (empty blue square, red diamond). The black dashed line is ponderomotive scaling, and the blue and red dotted lines the modified scaling. (c) Typical electron spatial profile (best focus and full energy). The blue dot and ring are laser axis and angular scale, white ring is the fitted Gaussian FWHM. Black regions were blocked by other diagnostics. (d) Experimental measurements of θ_e against I_L for changing r_L (blue circles) or E_L (red circles), typical experimental uncertainty (black cross) and linear fits to guide the eye (dashed).

FIG. 1. (a) Experimental setup and (b) simulated prepulse-driven target expansion in different conditions 10 ps before main pulse.

to or smaller than observations for longer pulse lasers at similar energies [64–66]. As shown in Fig. 2(d), lowering I_L by increasing r_L results in increased electron divergence, contrasting with previous measurements at lower intensities and larger focal spots [67]. However, using a tight focus and varying I_L by changing E_L showed little variation, indicating a process inherent to the laser geometry. Therefore, we have shown a spot size dependence on both electron temperature and divergence.

The impact of r_L has not previously appeared in electron heating models. For an electron in a plane wave, the characteristic transverse and longitudinal acceleration length, $y_0 \propto a_0$ and $x_0 \propto a_0^2$, can exceed the focal size bounded by $r_L \sim \lambda_L$ and Rayleigh length $x_R \sim \pi \lambda_L$ typical of high intensity lasers. Electron energy gain, given by the work done by the transverse electric field $W_y = -\int_c |e| E_y dy$, can therefore be suppressed due to insufficient acceleration length.

However, actual field distributions are complicated by focusing, reflection, and plasma effects. It has been shown that longitudinal oscillating electric fields [68,69] or static plasma magnetic [70] and electric fields [71,72] affect electron heating. Therefore, particle-in-cell (PIC) simulations were performed using EPOCH2D [73]. A box of $60 \times 60~\mu m$ was simulated with spatial resolution 10×20 nm. A $\tau_L = 40$ fs laser was focused on the target with varied r_L and I_L using p polarization unless otherwise specified. The target was $d = 5~\mu m$ preionized iron at $45°$ angle of incidence, with 50(4) particles per cell for electrons(ions). To minimize numerical heating, the peak target electron density was restricted to $250n_c$, still significantly higher than n_{cr}. To isolate the electron acceleration physics, the same preplasma conditions were used for all simulations described below [Fig. 1(b) blue line]. Additional simulations using the preplasma profiles from Fig. 1(b) showed variation in T_e of <10%.

The focal region is shown in Fig. 3(a) for best focus conditions ($r_L = 1.5~\mu m$, $I_L = 5 \times 10^{21}$ W cm^{-2}). The laser penetrates the preplasma and is reflected at the relativistic critical density $n_e \approx n_{cr}$, with no appreciable self-focusing. The electrons within the focal spot are driven along the laser axis and generate a strong azimuthal magnetic field $\bar{B}_z > 40$ kT [74]. This pinching field is even more evident in simulations with the laser polarization rotated out-of-plane (s-pol.). As evidenced by the overlaid electron trajectories, forward accelerated electrons are reflected by this field towards the laser axis [75], reducing their divergence [18,76]. The electron distribution is exponential above >5 MeV, and fitting a temperature at the pulse peak including all simulation particles, gives $T_e \approx 11$ MeV, significantly less than $T_{pond} \approx 24$ MeV and matching the experimental observation.

Increasing r_L with fixed intensity causes T_e to increase until it reaches the ponderomotive scaling [Fig. 3(b), blue circles]. Despite the same field strength, using a small focus
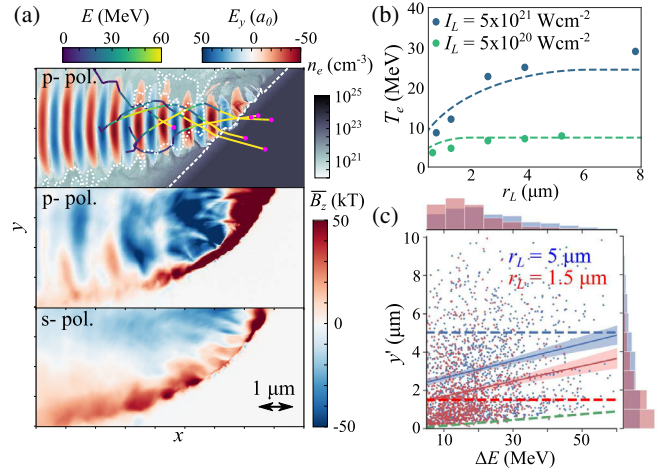

FIG. 3. From PIC: (a) n_e and E_y (visible where $a_0 > 10$) at the pulse peak, with dotted and dashed lines representing n_c and $n_{cr} = a_0 n_c$, respectively, and representative electron traces overlaid (top). Laser-cycle averaged magnetic field $\bar{B}_z$ for simulations with p and s polarization (middle and bottom). (b) T_e against r_L for two values of I_L, and respective model prediction [dotted line, Eq. (1)]. (c) y' against ΔE for $I_L = 6 \times 10^{20}$ W cm^{-2} and $r_L = 1.5, 5~\mu m$ of 1300 traced electrons > 5 MeV (red, blue respectively). The dashed lines are the respective focal spot sizes, solid lines are a linear regression fit, and the green dashed line is y'_{min}.

has affected not just the number, but also the average kinetic energy of the electrons. Suppression of T_e at small focal spots is also apparent at lower intensities [5×10^{20} W cm^{-2} Fig. 3(b), green circles], agreeing with the model [Eq. (1)]. Further simulations varying focal spot size and energy over the experimental range are shown in Fig. 2(b), reproducing the trend. As the focal spot increases, the azimuthal magnetic field which reduced the electron divergence at small r_L [Fig. 3(b)] weakens due to decreasing current density and increase in focal size to much larger than the preplasma spatial scale. The resultant electron momentum distribution extends to larger angles, also seen experimentally.

Following individual electron trajectories shows that the complex field pattern at the front surface results in rapidly varying accelerating trajectories, with most electrons experiencing semistochastic accelerating phases before entering the target [77]. On average, the majority of work was done by the transverse field [>80%–90%, depending on focusing geometry (see Supplemental Material [49] for more detail), depending on focusing geometry], therefore electrons require a transverse acceleration length $y' = \int |v_y| dt$ to gain energy. In Fig. 3(c), y' during acceleration (defined as when $5m_e c^2 < E < E_{max}$), is plotted against electron energy gain ΔE for two different focal sizes for $I_L = 6 \times 10^{20}$ W cm^{-2}, showing strong positive correlation. The most energetic electrons are accelerated over a path significantly larger than the minimum

$y'_{\min} = \Delta E/eE_L$ (green dashes). As indicated by the histograms, the smaller focal spot leads to lower acceleration lengths, despite the self-generated azimuthal field, and therefore lower energies.

Although describing average electron dynamics in such a complex field pattern is analytically challenging, a heuristic model based on ponderomotive scaling can replicate the observed T_e. For a plane wave, an electron has a maximum transverse momentum $p_y = a_0 m_e c$ and transverse acceleration distance $y_0 = a_0 \lambda_L/2\pi$. In the ponderomotive model [15], the electron temperature is set to the transverse kinetic energy of the electron, $T_e = [\sqrt{1 + (p_y/m_e c)^2} - 1]m_e c^2$. Instead, if acceleration ceases at $y = r_{Le}$, where $r_{Le} = r_L/(2\sqrt{\ln 2})$ is the radius where the intensity reduces by $1/e$, then by rewriting p_y in terms of y and setting $p_y = y = 0$ before acceleration, the final momentum at $y = r_{Le}$ is

$$p_f = a_0 m_e c \left[1 - \left(1 - \frac{r_{Le}}{y_0}\right)^2\right]^{1/2} \tag{1}$$

for $r_{Le} < y_0$. When $r_{Le} > y_0$, there is no restriction by the field size and $p_f = a_0 m_e c$; however, for $r_{Le} \ll y_0$ the momentum saturates. Using $p_y = p_f$ for calculating T_e predicts the saturation of T_e and the r_L dependence seen experimentally [dotted lines Fig. 2(b)] and numerically [dashes Fig. 3(b)].

An important application of electron heating in laser-solid interactions is ion acceleration in the surface sheath, which depends on the electron source parameters discussed above. The maximum proton energy E_p against E_L ($r_L \approx 1.5$ μm) and r_L ($E_L \approx 10$ J) is plotted in Figs. 4(a) and 4(b). Increasing E_L shows an approximate power law scaling $E_p \propto E_L^{0.6} \propto I_L^{0.6}$, weaker than observed previously at lower laser energy for ~fs lasers [43]. However, increasing intensity by decreasing r_L shows even weaker scaling, $E_p \propto r_L^{-1/2} \propto I_L^{1/4}$. Focusing to $r_L < 5$ μm has neither increased T_e, nor significantly boosted the maximum proton energy E_p despite increasing I_L.
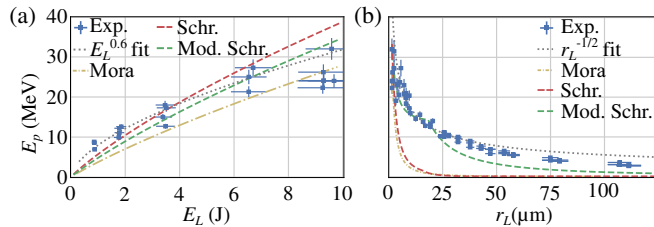

FIG. 4. (a) E_p against E_L for energy scan and (b) r_L for focal scan. Gray dots represent $E_L^{0.6}$ and $r_L^{-1/2}$ power law fits, yellow, red, and green dashes are the Mora, Schreiber, and modified models, respectively. Error bars are from uncertainty in laser parameters and TOF accuracy.

These observations were compared to widely used sheath models. The Mora model [36] was calculated following the assumptions in Ref. [38] except for T_e and θ_e which were taken from experimental data (Fig. 2) and using conversion efficiencies of laser energy into electrons $\eta = 0.07$ as a free variable to fit maximum proton energy at best focus (Fig. 4). This η is significantly lower than expected for such high intensities, and the validity of an isothermal approximation for ~fs lasers is doubtful [78]. We also plot the Schreiber model, which assumes a quasistatic potential generated by a finite size surface charge of radius $R = r + d\tan\theta$ on the target surface [42], where $r = r_L/\sqrt{2\ln 2}$ is the focus radius ($1/e^2$) and $\theta = \theta_e/2\sqrt{\ln 2}$ is the electrons half-angle ($1/e$). The predictions of the model are shown with the red dashed line in Figs. 4(a), 4(b), using $\tau_L = 40$ fs, $d = 5$ μm, and θ_E from the linear fits in Fig. 2(d). The laser energy input to the model is $E'_L = SE_L$ where S is the experimental Strehl ratio $S \approx 0.5$ [46] to include the difference in fluence between the experimental and diffraction limited spot, i.e., not all laser energy is usefully focused. We apply the widely used scaling $\eta = 1.2 \times 10^{-15} I_L^{3/4}$ (W cm^{-2}) up to a maximum $\eta = 0.5$ [38,42,79,80], using the experimentally inferred I_L (the discontinuity at $\eta = 0.5$ also causes a discontinuity in the model). Despite these assumptions, the model reasonably reproduces the E_L scan in Fig. 4(a) without free variables, demonstrating its appropriateness for tightly focused spots. However, both models severely underestimate E_p for larger focal spots [Fig. 4(b)].

This model assumes electrons only contribute once to the sheath, accelerating ions during a time $\tau = \tau_L$ over which the equation of motion is integrated [42]. However, electrons recirculating between the front and rear surfaces can increase the accelerating potential [81,82]. For small sheath size R, the recirculating electrons are unlikely to reappear within the same area. However, for larger R, recirculated electrons can contribute to the sheath. Considering an average electron velocity perpendicular to the target $v_{eT} \approx c/2$, they escape after $\tau_{esc} \approx 2R/c$, resulting in an acceleration time calculated by adding in quadrature $\tau = \sqrt{\tau_L^2 + \tau_{esc}^2}$ [40]. Furthermore, the sheath size is modified due to the 45° angle of incidence to $R' \approx r + \sqrt{2}d\tan\theta$, reducing the sheath potential for small r_L. The resulting estimates are plotted in Fig. 4 (red dashes), resulting in agreement over 3 orders of magnitude in intensity. This energy enhancement for large spots leads to weak E_p scaling with reducing r_L. We note that for current fs-class lasers, timescales are too short for magnetic fields to suppress ion energies [83]. Although our demonstration of proton beams up to 30 MeV at 0.1 Hz is promising for midenergy applications, generation of higher energies for applications such as radiotherapy using sheath acceleration requires increased laser energy, motivating research into alternative acceleration schemes.

To conclude, due to insufficient acceleration length at ultrahigh intensities we observed a focal-spot dependent saturation of electron temperature. The resultant sheath accelerated protons showed weak energy scaling when increasing intensity by tightly focusing due to a decrease in effective acceleration time. Therefore, we have demonstrated fundamental limitations of using very tightly focused spots in ultraintense laser-solid interactions. Deviations from scaling laws are important for applications using lasers operating at the high-intensity frontier.

---

[*] dover.nicholas@qst.go.jp

[1] H. Daido, M. Nishiuchi, and A. S. Pirozhkov, Rep. Prog. Phys. **75**, 056401 (2012).

[2] A. Macchi, M. Borghesi, and M. Passoni, Rev. Mod. Phys. **85**, 751 (2013).

[3] C. M. Brenner, S. R. Mirfayzi, D. R. Rusby, C. Armstrong, A. Alejo, L. A. Wilson, R. Clarke, H. Ahmed, N. M. H. Butler, D. Haddock *et al.*, Plasma Phys. Controlled Fusion **58**, 014039 (2016).

[4] M. Tabak, J. Hammer, M. E. Glinsky, W. L. Kruer, S. C. Wilks, J. Woodworth, E. M. Campbell, M. D. Perry, and R. J. Mason, Phys. Plasmas **1**, 1626 (1994).

[5] R. Kodama, P. A. Norreys, K. Mima, A. E. Dangor, R. G. Evans, H. Fujita, Y. Kitagawa, K. Krushelnick, T. Miyakoshi, N. Miyanaga *et al.*, Nature (London) **412**, 798 (2001).

[6] M. Roth, T. E. Cowan, M. H. Key, S. P. Hatchett, C. Brown, W. Fountain, J. Johnson, D. M. Pennington, R. A. Snavely, S. C. Wilks *et al.*, Phys. Rev. Lett. **86**, 436 (2001).

[7] A. Yogo, K. Sato, M. Nishikino, M. Mori, T. Teshima, H. Numasaki, M. Murakami, Y. Demizu, S. Akagi, S. Nagayama *et al.*, Appl. Phys. Lett. **94**, 181502 (2009).

[8] D. Doria, K. F. Kakolee, S. Kar, S. K. Litt, F. Fiorini, H. Ahmed, S. Green, J. C. G. Jeynes, J. Kavanagh, D. Kirby *et al.*, AIP Adv. **2**, 011209 (2012).

[9] B. Dromey, M. Coughlan, L. Senje, M. Taylor, S. Kuschel, B. Villagomez-Bernabe, R. Stefanuik, G. Nersisyan, L. Stella, J. Kohanoff *et al.*, Nat. Commun. **7**, 10642 (2016).

[10] M. Barberio, M. Scisciò, S. Vallières, F. Cardelli, S. N. Chen, G. Famulari, T. Gangolf, G. Revet, A. Schiavi, M. Senzacqua, and P. Antici, Nat. Commun. **9**, 372 (2018).

[11] G. A. Mourou, T. Tajima, and S. V. Bulanov, Rev. Mod. Phys. **78**, 309 (2006).

[12] M. Roth, D. Jung, K. Falk, N. Guler, O. Deppert, M. Devlin, A. Favalli, J. Fernandez, D. Gautier, M. Geissel *et al.*, Phys. Rev. Lett. **110**, 044802 (2013).

[13] C. Danson, D. Hillier, N. Hopps, and D. Neely, High Power Laser Sci. Eng. **3**, e3 (2015).

[14] A. Di Piazza, C. Müller, K. Z. Hatsagortsyan, and C. H. Keitel, Rev. Mod. Phys. **84**, 1177 (2012).

[15] S. C. Wilks, W. L. Kruer, M. Tabak, and A. B. Langdon, Phys. Rev. Lett. **69**, 1383 (1992).

[16] T. Kluge, T. Cowan, A. Debus, U. Schramm, K. Zeil, and M. Bussmann, Phys. Rev. Lett. **107**, 205003 (2011).

[17] J. D. Lindl and P. K. Kaw, Phys. Fluids **14**, 371 (1971).

[18] Y. Sentoku, K. Mima, H. Ruhl, Y. Toyama, R. Kodama, and T. E. Cowan, Phys. Plasmas **11**, 3083 (2004).

[19] A. Sorokovikova, A. V. Arefiev, C. McGuffey, B. Qiao, A. P. L. Robinson, M. S. Wei, H. S. McLean, and F. N. Beg, Phys. Rev. Lett. **116**, 155001 (2016).

[20] M. I. K. Santala, M. Zepf, I. Watts, F. N. Beg, E. Clark, M. Tatarakis, K. Krushelnick, A. E. Dangor, T. McCanny, I. Spencer *et al.*, Phys. Rev. Lett. **84**, 1459 (2000).

[21] R. J. Gray, D. C. Carroll, X. H. Yuan, C. M. Brenner, M. Burza, M. Coury, K. L. Lancaster, X. X. Lin, Y. T. Li, D. Neely *et al.*, New J. Phys. **16**, 113075 (2014).

[22] M. G. Haines, M. S. Wei, F. N. Beg, and R. B. Stephens, Phys. Rev. Lett. **102**, 045008 (2009).

[23] F. N. Beg, A. R. Bell, A. E. Dangor, C. N. Danson, A. P. Fews, M. E. Glinsky, B. A. Hammel, P. Lee, P. A. Norreys, and M. Tatarakis, Phys. Plasmas **4**, 447 (1997).

[24] R. A. Snavely, M. H. Key, S. P. Hatchett, T. E. Cowan, M. Roth, T. W. Phillips, M. A. Stoyer, E. A. Henry, T. C. Sangster, M. S. Singh *et al.*, Phys. Rev. Lett. **85**, 2945 (2000).

[25] E. L. Clark, K. Krushelnick, M. Zepf, F. N. Beg, M. Tatarakis, A. Machacek, M. I. K. Santala, I. Watts, P. A. Norreys, and A. E. Dangor, Phys. Rev. Lett. **85**, 1654 (2000).

[26] M. Nishiuchi, H. Sakaki, T. Zh. Esirkepov, K. Nishio, T. A. Pikuz, A. Ya. Faenov, I. Y. Skobelev, R. Orlandi, H. Sako, A. S. Pirozhkov *et al.*, Phys. Plasmas **22**, 033107 (2015).

[27] J. Schreiber, P. R. Bolton, and K. Parodi, Rev. Sci. Instrum. **87**, 071101 (2016).

[28] T. Esirkepov, M. Borghesi, S. V. Bulanov, G. Mourou, and T. Tajima, Phys. Rev. Lett. **92**, 175003 (2004).

[29] A. P. L. Robinson, M. Zepf, S. Kar, R. G. Evans, and C. Bellei, New. J. Phys. **10**, 013021 (2008).

[30] J. Denavit, Phys. Rev. Lett. **69**, 3052 (1992).

[31] L. O. Silva, M. Marti, J. R. Davies, R. A. Fonseca, C. Ren, F. S. Tsung, and W. B. Mori, Phys. Rev. Lett. **92**, 015002 (2004).

[32] F. Fiuza, A. Stockem, E. Boella, R. A. Fonseca, L. O. Silva, D. Haberberger, S. Tochitsky, C. Gong, W. B. Mori, and C. Joshi, Phys. Rev. Lett. **109**, 215001 (2012).

[33] L. Yin, B. J. Albright, B. M. Hegelich, and J. C. Fernández, Laser Part. Beams **24**, 291 (2006).

[34] A. Henig, D. Kiefer, K. Markey, D. C. Gautier, K. A. Flippo, S. Letzring, R. P. Johnson, T. Shimada, L. Yin, B. J. Albright *et al.*, Phys. Rev. Lett. **103**, 045002 (2009).

[35] S. Palaniyappan, C. Huang, D. C. Gautier, C. E. Hamilton, M. A. Santiago, C. Kreuzer, A. B. Sefkow, R. C. Shah, and J. C. Fernández, Nat. Commun. **6**, 10170 (2015).

[36] P. Mora, Phys. Rev. Lett. **90**, 185002 (2003).

[37] P. Mora, Phys. Rev. E **72**, 056401 (2005).

[38] J. Fuchs, P. Antici, E. D'Humières, E. Lefebvre, M. Borghesi, E. Brambrink, C. A. Cecchetti, M. Kaluza, V. Malka, M. Manclossi *et al.*, Nat. Phys. **2**, 48 (2006).

[39] M. Passoni, L. Bertagna, and A. Zani, New J. Phys. **12**, 045012 (2010).

[40] C. M. Brenner, P. McKenna, and D. Neely, Plasma Phys. Controlled Fusion **56**, 084003 (2014).

[41] L. Robson, P. T. Simpson, R. J. Clarke, K. W. D. Ledingham, F. Lindau, O. Lundh, T. McCanny, P. Mora, D. Neely, C.-G. Wahlström *et al.*, Nat. Phys. **3**, 58 (2007).

[42] J. Schreiber, F. Bell, F. Grüner, U. Schramm, M. Geissler, M. Schnürer, S. Ter-Avetisyan, B. M. Hegelich, J. Cobble, E. Brambrink *et al.*, Phys. Rev. Lett. **97**, 045005 (2006).

[43] K. Zeil, S. D. Kraft, S. Bock, M. Bussmann, T. E. Cowan, T. Kluge, J. Metzkes, T. Richter, R. Sauerbrey, and U. Schramm, New J. Phys. **12**, 045015 (2010).

[44] D. T. Offermann, K. A. Flippo, J. Cobble, M. J. Schmitt, S. A. Gaillard, T. Bartal, D. V. Rose, D. R. Welch, M. Geissel, and M. Schollmeier, Phys. Plasmas **18**, 056713 (2011).

[45] B. Aurand, L. Senje, K. Svensson, M. Hansson, A. Higginson, A. Gonoskov, M. Marklund, A. Persson, O. Lundh, D. Neely *et al.*, Phys. Plasmas **23**, 023113 (2016).

[46] A. S. Pirozhkov, Y. Fukuda, M. Nishiuchi, H. Kiriyama, A. Sagisaka, K. Ogura, M. Mori, M. Kishimoto, H. Sakaki, N. P. Dover *et al.*, Opt. Express **25**, 20486 (2017).

[47] H. Kiriyama, A. S. Pirozhkov, M. Nishiuchi, Y. Fukuda, K. Ogura, A. Sagisaka, Y. Miyasaka, M. Mori, H. Sakaki, N. P. Dover *et al.*, Opt. Lett. **43**, 2595 (2018).

[48] M. Nishiuchi, H. Kiriyama, H. Sakaki, N. P. Dover, K. Kondo, A. S. Pirozhkov, A. Sagisaka, Y. Fukuda, K. Nishitani, T. Miyahara *et al.*, Proc. SPIE Int. Soc. Opt. Eng. **10241** (2017).

[49] See Supplemental Material at http://link.aps.org/supplemental/10.1103/PhysRevLett.124.084802 for more details of the laser and diagnostic setup, which includes Refs. [46,50–60] and for more description of the FLASH simulation setup, which includes Refs. [61–63].

[50] H. Sakaki *et al.* (to be published).

[51] L. Gremillet, G. Bonnaud, and F. Amiranoff, Phys. Plasmas **9**, 941 (2002).

[52] M. S. Wei, F. N. Beg, E. L. Clark, A. E. Dangor, R. G. Evans, A. Gopal, K. W. D. Ledingham, P. McKenna, P. A. Norreys, M. Tatarakis *et al.*, Phys. Rev. E **70**, 056412 (2004).

[53] M. Manclossi, J. J. Santos, D. Batani, J. Faure, A. Debayle, V. T. Tikhonchuk, and V. Malka, Phys. Rev. Lett. **96**, 125002 (2006).

[54] C. M. Huntington, A. G. R. Thomas, T. Matsuoka, V. Chvykov, G. Kalintchenko, S. Kneip, Z. Najmudin, C. Palmer, V. Yanovsky, A. Maksimchuk *et al.*, Phys. Rev. Lett. **106**, 105001 (2011).

[55] J. Peebles, A. V. Arefiev, S. Zhang, C. McGuffey, M. Spinks, J. Gordon, E. W. Gaul, G. Dyer, M. Martinez, M. E. Donovan *et al.*, Phys. Rev. E **98**, 053202 (2018).

[56] S. Nakamura, Y. Iwashita, A. Noda, T. Shirai, H. Tongu, A. Fukumi, M. Kado, A. Yogo, M. Mori, and S. Orimo, Jpn. J. Appl. Phys. **45**, L913 (2006).

[57] K. Nemoto, A. Maksimchuk, S. Banerjee, K. Flippo, G. Mourou, D. Umstadter, and V. Yu. Bychenkov, Appl. Phys. Lett. **78**, 595 (2001).

[58] J. Fuchs, Y. Sentoku, S. Karsch, J. Cobble, P. Audebert, A. Kemp, A. Nikroo, P. Antici, E. Brambrink, A. Blazevic *et al.*, Phys. Rev. Lett. **94**, 045004 (2005).

[59] N. P. Dover, M. Nishiuchi, H. Sakaki, M. A. Alkhimova, A. Ya. Faenov, Y. Fukuda, H. Kiriyama, A. Kon, K. Kondo, K. Nishitani *et al.*, Rev. Sci. Instrum. **88**, 073304 (2017).

[60] M. Schollmeier, M. Geissel, A. B. Sefkov, and K. A. Flippo, Rev. Sci. Instrum. **85**, 043305 (2014).

[61] S. Faik, A. Tauschwitz, and I. Iosilevskiy, Comput. Phys. Commun. **227**, 117 (2018).

[62] R. M. More, K. H. Warren, D. A. Young, and G. B. Zimmerman, Phys. Fluids **31**, 3059 (1988).

[63] A. J. Kemp and J. Meyer-ter-Vehn, Nucl. Instrum. Methods Phys. Res., Sect. A **415**, 674 (1998).

[64] J. J. Santos, F. Amiranoff, S. D. Baton, L. Gremillet, M. Koenig, E. Martinolli, M. Rabec Le Gloahec, C. Rousseaux, D. Batani, A. Bernardinello *et al.*, Phys. Rev. Lett. **89**, 025001 (2002).

[65] J. Fuchs, T. E. Cowan, P. Audebert, H. Ruhl, L. Gremillet, A. Kemp, M. Allen, A. Blazevic, J.-C. Gauthier, M. Geissel *et al.*, Phys. Rev. Lett. **91**, 255002 (2003).

[66] M. Coury, D. C. Carroll, A. P. L. Robinson, X. H. Yuan, C. M. Brenner, M. Burza, R. J. Gray, M. N. Quinn, K. L. Lancaster, Y. T. Li *et al.*, Appl. Phys. Lett. **100**, 074105 (2012).

[67] J. S. Green, V. M. Ovchinnikov, R. G. Evans, K. U. Akli, H. Azechi, F. N. Beg, C. Bellei, R. R. Freeman, H. Habara, R. Heathcote *et al.*, Phys. Rev. Lett. **100**, 015003 (2008).

[68] L. Willingale, A. V. Arefiev, G. J. Williams, H. Chen, F. Dollar, A. U. Hazi, A. Maksimchuk, M. J.-E. Marley, W. Nazarov, T. Z. Zhao, and C. Zulick, New J. Phys. **20**, 093024 (2018).

[69] Z. Gong, A. P. L. Robinson, X. Q. Yan, and A. V. Arefiev, Plasma Phys. Controlled Fusion **61**, 035012 (2019).

[70] Z. Gong, F. Mackenroth, T. Wang, X. Q. Yan, T. Toncian, and A. V. Arefiev, arXiv:1811.00425.

[71] A. V. Arefiev, V. N. Khudik, A. P. L. Robinson, G. Schvets, L. Willingale, and M. Schollmeier, Phys. Plasmas **23**, 056704 (2016).

[72] V. Khudik, A. Arefiev, X. Zhang, and G. Schvets, Phys. Plasmas **23**, 103108 (2016).

[73] T. D. Arber, K. Bennett, C. S. Brady, A. Lawrence-Douglas, M. G. Ramsay, N. J. Sircombe, P. Gillies, R. G. Evans, H. Schmitz, A. R. Bell, and C. P. Ridgers, Plasma Phys. Controlled Fusion **57**, 113001 (2015).

[74] D. J. Stark, T. Toncian, and A. V. Arefiev, Phys. Rev. Lett. **116**, 185003 (2016).

[75] T. Kluge, S. A. Gaillard, K. A. Flippo, T. Burris-Mog, W. Enghardt, B. Gall, M. Geissel, A. Helm, S. D. Kraft, T. Lockard *et al.*, New J. Phys. **14**, 023038 (2012).

[76] H. Habara, K. Adumi, T. Yabuuchi, T. Nakamura, Z. L. Chen, M. Kashihara, R. Kodama, K. Kondo, G. R. Kumar, L. A. Lei *et al.*, Phys. Rev. Lett. **97**, 095004 (2006).

[77] L. Chopineau, A. Leblanc, G. Blaclard, A. Denoeud, M. Thévenet, J.-L. Vay, G. Bonnaud, Ph. Martin, H. Vincenti, and F. Quéré, Phys. Rev. X **9**, 011050 (2019).

[78] K. Zeil, J. Metzkes, T. Kluge, M. Bussmann, T. E. Cowan, S. D. Kraft, R. Sauerbrey, and U. Schramm, Nat. Commun. **3**, 874 (2012).

[79] M. H. Key, M. D. Cable, T. E. Cowan, K. G. Estabrook, B. A. Hammel, S. P. Hatchett, E. A. Henry, D. E. Hinkel, J. D. Kilkenny, J. A. Koch *et al.*, Phys. Plasmas **5**, 1966 (1988).

[80] J. Yu, Z. Jiang, J. C. Kieffer, and A. Krol, Phys. Plasmas **6**, 1318 (1999).

[81] A. J. Mackinnon, Y. Sentoku, P. K. Patel, D. W. Price, S. Hatchett, M. H. Key, C. Andersen, R. Snavely, and R. R. Freeman, Phys. Rev. Lett. **88**, 215006 (2002).

[82] S. Buffechoux, J. Psikal, M. Nakatsutsumi, L. Romagnani, A. Andreev, K. Zeil, M. Amin, P. Antici, T. Burris-Mog, A. Compant-La-Fontaine *et al.*, Phys. Rev. Lett. **105**, 015005 (2010).

[83] M. Nakatsutsumi, Y. Sentoku, A. Korzhimanov, S. N. Chen, S. Buffechoux, A. Kon, B. Atherton, P. Audebert, M. Geissel, L. Hurd *et al.*, Nat. Commun. **9**, 280 (2018).